Available online at www.sciencedirect.com
ScienceDirect
Journal of Catalysis 246 (2007) 166–176
JOURNAL OF CATALYSIS
www.elsevier.com/locate/jcat

VPO catalysts supported on H_3PO_4-treated ZrO_2 highly active for *n*-butane oxidation

Ru-Ming Feng [a,b], Xiu-Juan Yang [a,b], Wei-Jie Ji [b,*], Yi Chen [b], Chak-Tong Au [a,*]

[a] *Department of Chemistry, Center for Surface Analysis and Research, Hong Kong Baptist University, Kowloon Tong, Hong Kong, China*
[b] *Key Laboratory of Mesoscopic Chemistry, Ministry of Education, School of Chemistry and Chemical Engineering, Nanjing 210093, China*

Received 3 October 2006; revised 22 November 2006; accepted 22 November 2006

Available online 4 January 2007

Abstract

VPO catalysts supported on ZrO_2 and H_3PO_4-treated ZrO_2 were prepared for the first time by means of precipitation–deposition in an organic medium. The physicochemical properties of the catalysts were investigated by the BET, XRD, TEM, Raman, XPS, and H_2-TPR techniques. It was found that the way of H_3PO_4 treatment conducted on ZrO_2 has a significant effect on the nature of the support, as well as on the state and structure of the VPO component loaded on it. The discrepancies in the synergistic interaction between VPO and the different supports induce variation in catalytic performance. The change in VPO loading is found to have an effect on catalyst efficiency. At 673 K, the MA yield is 61 mol% over the 36%VPO/(H_3PO_4)-*p*-ZrO_2 catalyst, the best performance achieved so far among the supported VPOs.

Keywords: H_3PO_4 treatment; ZrO_2; Supported VPO; *n*-Butane oxidation; Maleic anhydride

1. Introduction

The partial oxidation of *n*-butane to maleic anhydride (MA) involves the transfer of a total of 14 electrons in a number of consecutive reaction steps [1]. Despite the complexity, the reaction is effectively catalyzed by vanadium phosphorus oxide (VPO) catalysts [2–6]. In fact, it is the only industrialized catalyst system used exclusively for the oxidation of light alkanes. Much effort has been devoted to advancing our understanding of these catalysts [6–12], including the functions of the active phases and the nature of active sites [13–30].

It could be advantageous to have the VPO catalysts supported in terms of better heat transfer, larger surface area to volume ratio of active component, better mechanical strength, and other properties, and materials including SiO_2, TiO_2, Al_2O_3, SiC, Al-containing MCM-41, and SBA-15 have been used as supports [31–40]. It has been recognized that the use of specific supports and preparation methods can have a significant effect on the nature and performance of a VPO catalyst [32,41, 42]. VPO catalysts prepared in an organic medium are known to perform better than those prepared in an aqueous solution [43]. *Iso*-butanol [9,19,44–48] and benzyl alcohol [24,49,50] have been adopted for generating VPO catalysts in an organic medium. It was reported that V^{5+}-containing phases such as α_1-$VOPO_4$ and γ-$VOPO_4$ were generated in supported VPO, especially when the catalyst was prepared in aqueous solution and that the presence of the α_1-$VOPO_4$ and γ-$VOPO_4$ phases in large amount would lower *n*-butane conversion and/or MA selectivity [21,35,51].

ZrO_2 is a versatile material that has been widely used as catalyst support or support component in applications such as (i) NO_x SCR with hydrocarbons [52], (ii) TWCs [53,54], (iii) methanol synthesis and decomposition [55–57], (iv) CO hydrogenation [58], (v) methane partial oxidation [59], (vi) methanol steam reforming [60,61], and (vii) sulfated ZrO_2 solid acids [62,63]. The literature contains a wide variety of materials that have been used to support VPO but not ZrO_2. To the best of our knowledge, the present study is the first time that ZrO_2 was adopted to support VPO. We studied the dispersion of VPO on ZrO_2, and investigated the effect of preparation methodology—

* Corresponding authors.
E-mail addresses: jiwj@nju.edu.cn (W.-J. Ji), pctau@hkbu.edu.hk (C.-T. Au).

0021-9517/$ – see front matter
doi:10.1016/j.jcat.2006.11.027

particularly the treatment of support with H_3PO_4—on the nature and performance of VPO.

2. Experimental

2.1. Catalyst preparation

The ZrO_2 material was prepared by mixing 4.0 g of $ZrOCl_2 \cdot 8H_2O$ and 1.0 g of CTAB in aqueous medium ($pH \geqslant 12$) at 70 °C and then via a hydrothermal procedure in an autoclave at 100 °C for 48 h. The resulted solid was dried at 373 K for 10 h, and is designated "dried precursor of ZrO_2" hereinafter. Before VPO loading, the dried precursor was calcined at 550 °C for 8 h and denoted as "calcined ZrO_2" before being used directly as support or subject to H_3PO_4 treatment (i.e., 1 g of ZrO_2/20 ml H_3PO_4 solution of 1 mol/L, at 70 °C, for 12 h). The filtered solid was washed repeatedly with D.I. water until the pH of filtering solution reached 7.0. For comparison, a portion of "dried precursor of ZrO_2" underwent the same H_3PO_4 treatment, and the resulting material was dried and calcined again, as described earlier before VPO loading.

The loading of VPO in mixed *iso*-butyl/benzyl alcohols was performed as described previously [40,64]. In brief, V_2O_5 was first refluxed in a mixture of *iso*-butyl/benzyl alcohols (volume ratio of 1:1) at 140 °C for 6 h. Subsequently, PEG 6000 and a particular support were introduced in suitable amounts. After 30 min, reaction temperature was lowered to 130 °C and phosphoric acid (85%) was added dropwise to reach a P/V atomic ratio of 1.2/1.0. After refluxing for another 7 h, the suspension was filtered, and the solid was washed with *iso*-butanol and acetone, respectively, and dried in air at 120 °C for 24 h. The powder was pressed into pellets, crushed, and sieved (40–60 mesh). The catalyst prepared by loading VPO on H_3PO_4-treated "dried precursor of ZrO_2" is designated VPO/(H_3PO_4)-*p*-ZrO_2, and that prepared by loading VPO on H_3PO_4-treated "calcined ZrO_2" is designated VPO/(H_3PO_4)-ZrO_2 hereinafter.

Before characterization and performance evaluation, all of the samples were subject to in situ activation. The sample was heated from room temperature (RT) to 400 °C at a rate of 2 °C/min in the reaction mixture (i.e., 1.5% *n*-butane/air), and kept at this temperature for at least 15 h. The freshly activated catalyst was gray in color.

2.2. Catalyst evaluation

The 0.5-g catalyst samples were evaluated for the partial oxidation of *n*-butane to MA in a quartz fixed-bed microreactor ($\Phi = 8$ mm) with a continuous reactant downflow. The feed composition was 1.5% *n*-C_4H_{10}, 17.5% O_2 (in volume), and balance N_2. The gas hourly space velocity (GHSV) was in the range of 1200–3000 h^{-1}. An on-line GC system was used to analyze the outlet effluent; the carbon balance was usually >95%.

2.3. Characterization

Powder X-ray diffraction was conducted using a Rigaku automatic diffractometer (Rigaku D-MAX) with monochromatized Cu$K\alpha$ radiation ($\lambda = 0.1541$ nm) at a setting of 30 kV. The BET surface area was measured using an ASPS-2100 instrument. The sample was outgassed at 300 °C for 3 h, after which N_2 adsorption was conducted at −196 °C. Raman spectra were collected using a LABRAM-HR Raman spectrometer at RT with excitation source of 513 nm and power of 1.0 mW. XPS measurement was performed using an X-ray photoelectron spectrometer (VG ESCALAB Mark II) with 1253.6 eV of Mg$K\alpha$ radiation at settings of 10 kV and 20 mA. The binding energies (BEs) were calibrated against the C 1s signal (284.6 eV) of contaminant carbon. The surface composition of elements was estimated on the basis of having the corresponding peak areas normalized according to the Wagner factor database. The TEM images were obtained with a TEM-200CX transmission electron microscope. Temperature-programmed reduction (TPR) was carried out in the temperature range of RT ∼ 900 °C. The sample was reduced in 5% H_2/Ar (40 ml/min) at a rate of 10 °C/min.

3. Results and discussion

3.1. Characterization

3.1.1. BET, TEM, and XRD

Despite the use of CTAB in an attempt to create mesopores in ZrO_2, the results of small-angle XRD and N_2 adsorption–desorption isotherms (not shown) suggest the absence of mesopores after calcination at 550 °C for 8 h. The specific surface areas of various samples are given in Table 1. H_3PO_4 treatment of "calcined ZrO_2" caused an increase in surface area from 27.0 to 35.7 m^2/g, whereas H_3PO_4-treatment of "dried precursor of ZrO_2" resulted in a slight decrease in surface area from 27.0 to 22.7 m^2/g. In the former case, increase in surface area is likely to be due to the partial dissolution of surface ZrO_2 by H_3PO_4 and the induced porosity on the support surface. Therefore, the method of H_3PO_4 treatment can have an affect on the texture of the supports. For the serial samples of VPO/(H_3PO_4)-*p*-ZrO_2, surface area decreases slightly with increasing VPO loading (Table 1). In addition, the surface areas of VPO/(H_3PO_4)-*p*-ZrO_2 samples are rather close to those of (H_3PO_4)-*p*-ZrO_2 support. The TEM images of the supports show grains of 200–300 nm (Fig. 1). H_3PO_4 treatment causes no obvious change in the size of the support particles (Fig. 1B). Nevertheless, the surface porosity of (H_3PO_4)-*p*-ZrO_2 (Fig. 1D) is enhanced compared with that of ZrO_2 (Fig. 1C). Dispersion of the VPO component on the (H_3PO_4)-*p*-ZrO_2 support is rather uniform (Fig. 1E), as illustrated in the close-up TEM image of 36%

Table 1
The specific surface areas of supports and selected supported VPO catalysts

Sample	S_{BET} (m^2/g)
ZrO_2	27.0
(H_3PO_4)-ZrO_2	35.7
(H_3PO_4)-*p*-ZrO_2	22.7
36% VPO/(H_3PO_4)-ZrO_2	22.8
27% VPO/(H_3PO_4)-*p*-ZrO_2	27.2
36% VPO/(H_3PO_4)-*p*-ZrO_2	24.2
45% VPO/(H_3PO_4)-*p*-ZrO_2	20.5

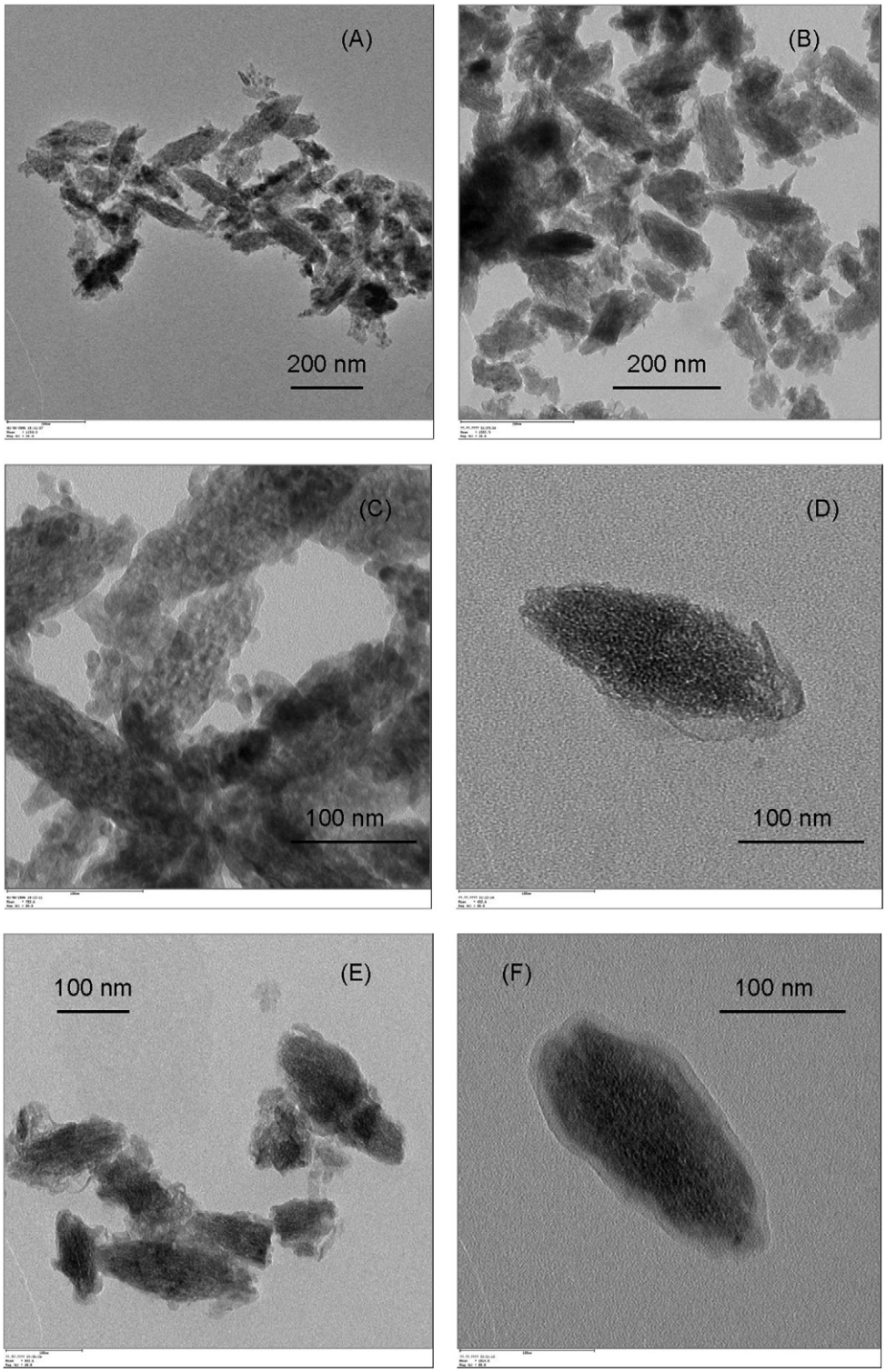

Fig. 1. Representative TEM images of (A) the dried ZrO_2 precursor; (B) the calcined (at 550 °C) H_3PO_4-*p*-ZrO_2 (H_3PO_4 concentration: 1 mol/L); (C) the close-up image of (A); (D) the close-up image of (B); (E) the activated 36% VPO/*p*-ZrO_2(H_3PO_4) catalyst; and (F) the close-up image of a particle of (E).

VPO/(H_3PO_4)-*p*-ZrO_2 (Fig. 1F). The results of TEM investigation are in good agreement with surface area measurements.

The wide-angle XRD patterns of samples with or without H_3PO_4-treatment, shown in Fig. 2, reveal that when the calcined ZrO_2 was used directly for VPO loading, the signal of $(VO)_2P_2O_7$ phase was hardly observed and the essential signal was that of monoclinic ZrO_2 [65] (Fig. 2A). The poor presence of $(VO)_2P_2O_7$ crystallite is similar to the case when VPO was supported on Al-containing MCM-41 [39]. It is apparent that the method of treating ZrO_2 by H_3PO_4 has an affect on VPO phase composition. Over VPO/(H_3PO_4)-*p*-ZrO_2, the XRD pattern indicates the presence of amorphous ZrO_2 and the predom-

inant $(VO)_2P_2O_7$ phase; the signals of the latter are similar to those of VPO supported on SBA-15 [40] and on fumed SiO_2 [64]. Over VPO/(H_3PO_4)-ZrO_2, the signals can be attributed to the phases of highly distorted monoclinic ZrO_2 and crystalline $(VO)_2P_2O_7$ species (minor) (Fig. 2A). We deduce that the treatment of H_3PO_4 not only suppresses the crystallization of the ZrO_2 precursor, thereby reducing ZrO_2 crystallinity, but also affects the state and structure of VPO species loaded on the support. Fig. 2B illustrates the effect of H_3PO_4 concentration adopted in H_3PO_4 treatment on phase composition of supported VPOs. It can be seen an increasing H_3PO_4 concentration enhances the vanadyl pyrophosphate phase. At 1.0 mol/L H_3PO_4 concentration, XRD signals of ZrO_2 diminish the most, suggesting a profound structural disorder (amorphous) of the support material. Over VPO/(H_3PO_4)-p-ZrO_2 catalysts, the intensity of $(VO)_2P_2O_7$ signals first increase at increasing VPO loading to 36% but then decline at a VPO loading of 45% (Fig. 2C), likely due to interaction between VPO and the support.

3.1.2. Raman

Fig. 3A gives the Raman spectra of pure VPO and samples of VPO supported on H_3PO_4-treated ZrO_2. The spectrum of unsupported VPO shows four well-resolved Raman bands at 928, 1036, 1136, and 1185 cm^{-1}. The major band at ca. 928 cm^{-1} can be attributed to ν(as) P–O–P in $P_2O_7^{2-}$ unit of $(VO)_2P_2O_7$, the weak bands at 1136 and 1185 cm^{-1} are characteristics of $(VO)_2P_2O_7$ species [9,10,22,51,64], and the band at 1036 cm^{-1} can be related to V^{5+}-containing species [19,22]. For the supported VPOs, the shoulders in the 950–970 cm^{-1} region indicate the coexistence of vanadyl pyrophosphate and orthophosphate (γ-$VOPO_4$, α_1-$VOPO_4$, and $VOPO_4{\cdot}2H_2O$) phases, and the bands at 1023, and 1030 cm^{-1} confirm the presence of V^{5+}-containing species in small proportion [9,10, 51,64]. In Fig. 3B, the impact of H_3PO_4 concentration on the VPO/(H_3PO_4)-p-ZrO_2 catalysts is obvious. At a H_3PO_4 concentration of 1.5 mol/L, and in terms of the intense bands at 926, 1123, and 1186 cm^{-1} as well as the noticeable bands at 1010 and 1043 cm^{-1}, enhanced formation and structural regularity of vanadyl pyrophosphate and orthophosphate phase are seen. At a H_3PO_4 concentration of 1.0 mol/L, the signal of V^{5+}-containing species in the range of 1000–1100 cm^{-1} is the lowest, and the structural regularity of the vanadyl pyrophosphate phase is also low because the intensity of the characteristic bands at 926, 1123, and 1186 cm^{-1} is notably decreased. Different from the silica-supported VPOs [51,64], the VPOs in the VPO/(H_3PO_4)-p-ZrO_2 catalysts exhibit declining Raman signals of vanadyl pyrophosphate species with a rise in VPO loading (Fig. 3C), suggesting possible interaction between VPO and support at high VPO loadings. All of the Raman observations are concordant with the XRD results.

3.1.3. H_2-TPR

Fig. 4A reports the reduction behaviors of the pure and supported VPO catalysts. For pure VPO sample, the TPR profile shows a main peak around 784 °C, attributable to the removal of lattice oxygen related to V^{4+} species in the $(VO)_2P_2O_7$ phase.

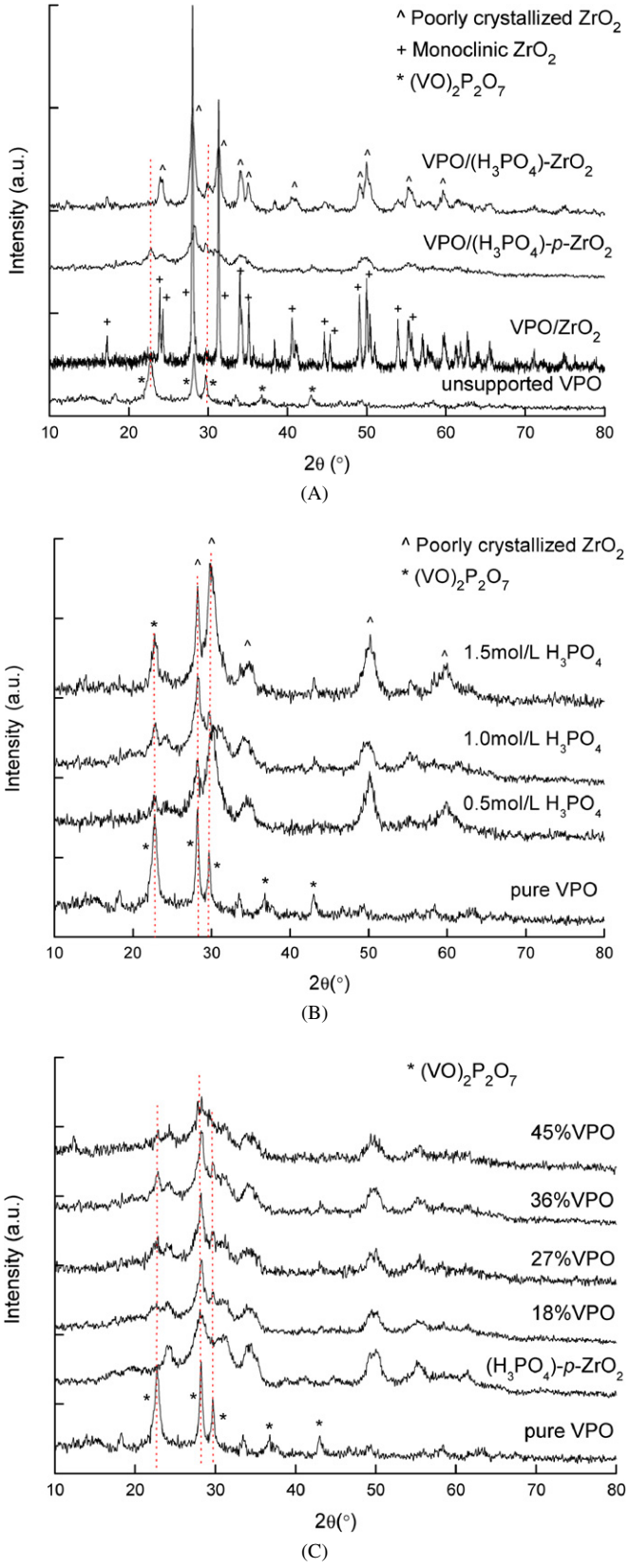

Fig. 2. The wide-angle XRD patterns of (A) different ZrO_2-supported VPOs (36 wt% loading) as well as unsupported VPO, (B) various VPO/(H_3PO_4)-p-ZrO_2 samples for which the support precursor was treated with different concentrations of H_3PO_4, and (C) the serial VPO/(H_3PO_4)-p-ZrO_2 samples with various VPO loadings as well as the unloaded (H_3PO_4)-p-ZrO_2 (H_3PO_4 concentration: 1 mol/L).

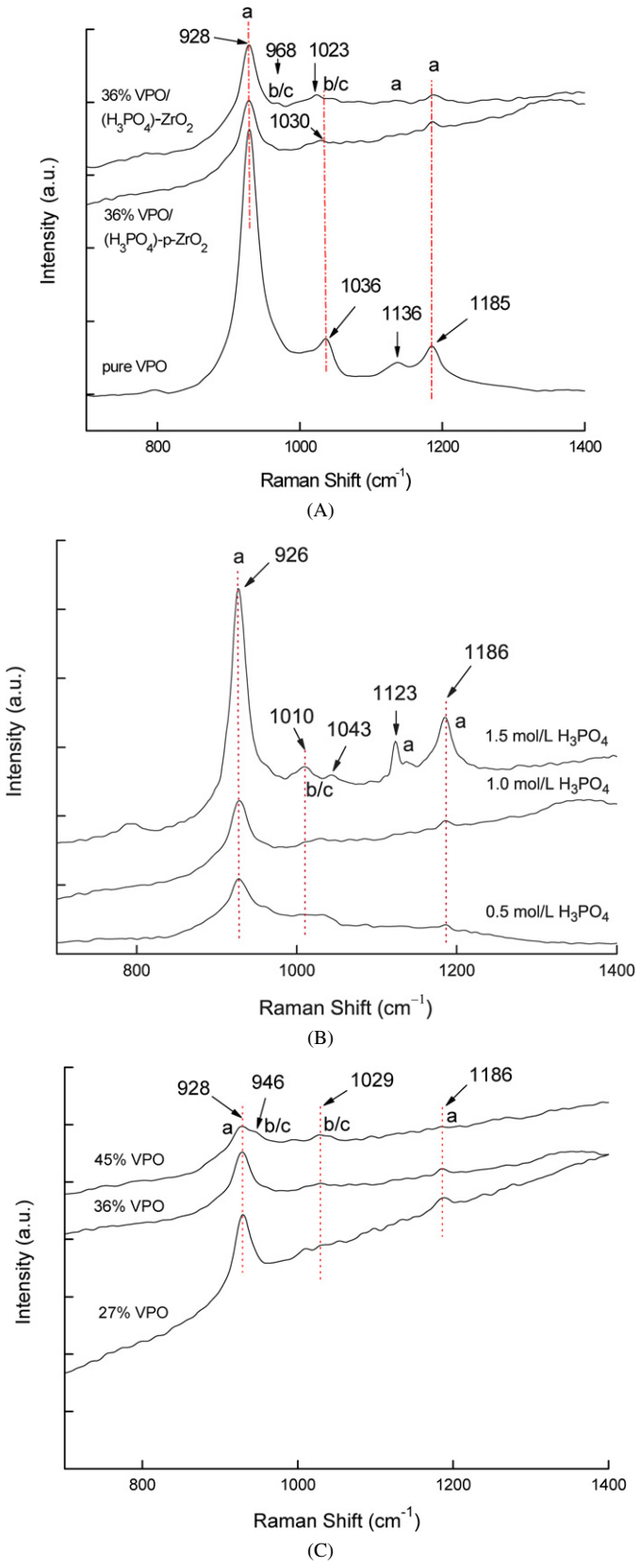

Fig. 3. Raman spectra of (A) supported VPOs (36% loading) as well as unsupported VPO, (B) the VPO/(H_3PO_4)-p-ZrO_2 samples for which the support precursor was treated with different concentrations of H_3PO_4, and (C) the serial VPO/(H_3PO_4)-p-ZrO_2 samples with different VPO loadings. (a) $(VO)_2P_2O_7$; (b) α_1-$VOPO_4$; (c) γ-$VOPO_4$.

The shoulder ranging from ca. 400 to 700 °C is attributed to the removal of lattice oxygen related to V^{5+} species [10,64]. Overall, the reduction behaviors of supported VPOs are strongly dependent on the history of support preparation/pretreatment. If "calcined ZrO_2" was used as support (in the case of 36% VPO/ZrO_2), the reduction of lattice oxygen related to V^{4+} species shifts toward higher temperature (800 °C), indicating that the lattice oxygen is relatively less reactive. The main reduction peak of 36% VPO/(H_3PO_4)-p-ZrO_2 is at 736 °C, whereas that of 36% VPO/(H_3PO_4)-ZrO_2 is at 770 °C, indicating that the former can be reduced more easily. As already mentioned, the shoulders in the ca. 400–700 °C range are owing to the reduction of V^{5+}-containing species. Based on peak areas, the amount of V^{5+} species in 36% VPO/ZrO_2 is the lowest and that in 36% VPO/(H_3PO_4)-ZrO_2 is the highest among the three supported VPOs. Previous studies indicated that the presence of certain amount of V^{5+} species in VPO catalysts was favorable for MA formation [15,21,24,27,64]; thus the 36% VPO/(H_3PO_4)-p-ZrO_2 sample containing a medium amount of V^{5+} species may function better for the reaction, and this is confirmed in the measurement of catalytic activity illustrated later in Section 3.2.

Shown in Fig. 4B are the influence of H_3PO_4 concentration adopted in H_3PO_4 treatment on the reduction behavior of the VPO/(H_3PO_4)-p-ZrO_2 samples. Despite the variation of H_3PO_4 concentration (0.5, 1.0, and 1.5 mol/L) shows no significant changes in the location of the main reduction peak (748, 738, and 752 °C, with that treated with H_3PO_4 of 1.0 mol/L the most reactive), its affect on the area of the main reduction peaks as well as the shoulders are obvious, suggesting that the relative contents of vanadyl pyrophosphate and orthophosphate species differ as related to the history of catalyst preparation, particularly H_3PO_4 treatment. The TPR results are in accordance with the Raman results described previously.

Fig. 4C presents the effect of VPO loading on the reduction behavior of the VPO component in the VPO/(H_3PO_4)-p-ZrO_2 samples. Note that the H_3PO_4-treated support material is essentially not reducible in the adopted temperature range. Compared with the main reduction peak of unsupported VPO, the main reduction peaks of the VPO/(H_3PO_4)-p-ZrO_2 samples occur at lower temperature. In other words, the lattice oxygen of the supported VPOs is higher in reactivity. With increasing VPO loading, the temperature of the main reduction peaks first increases (from 18 to 27% loading) and then decreases (from 27 to 45% loading). This trend reflects the extent of VPO–support interaction. Note that at the highest VPO loading of 45%, there is a broad and intense shoulder, suggesting the presence of orthophosphate species in relatively larger proportions.

3.1.4. XPS

As shown in Table 1, the V $2p_{3/2}$ BEs of the bulk VPO and supported VPO samples are in the range of 516.8–517.2 eV, close to the value of 517.6 eV reported for well-crystallized $(VO)_2P_2O_7$ [1,10,66,67] but lower than that reported for vanadium pentoxide and V(IV) phosphate [1,68]. Therefore, the vanadium oxidation states of these catalysts are approximately 4+, and the VPO components are mainly in the form of

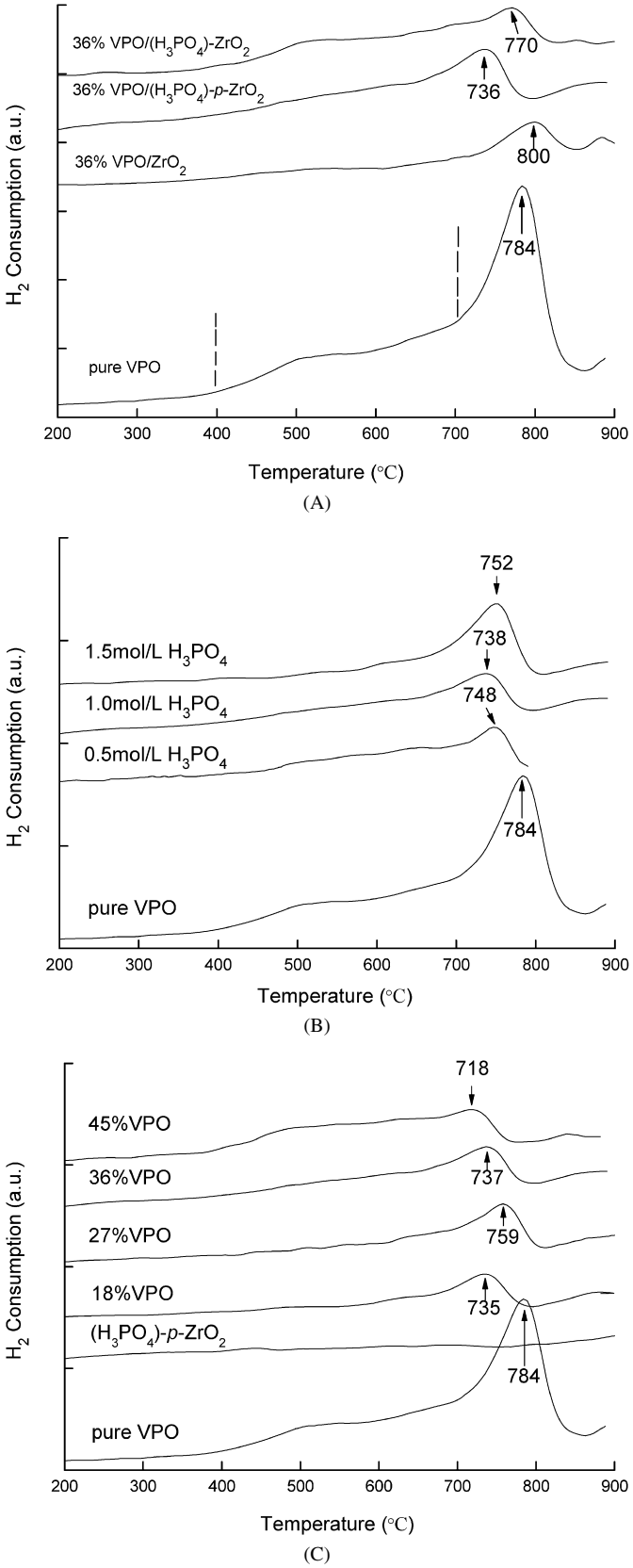

Fig. 4. Temperature-programmed reduction (TPR) profiles of (A) the supported VPOs with 36% loading as well as unsupported one, (B) the VPO/(H_3PO_4)-p-ZrO_2 samples for which the support precursor was treated with different concentrations of H_3PO_4, and (C) the serial VPO/(H_3PO_4)-p-ZrO_2 samples with different VPO loadings.

$(VO)_2P_2O_7$. The trend of V $2p_{3/2}$ BEs in the sample serial is also in accordance with the content of V^{5+}-containing species revealed by Raman and TPR investigations. The O 1s BEs of supported VPO catalysts are essentially the same as those of the unsupported VPO catalysts (ca. 531.3 eV). The P 2p BEs of supported and bulk VPO samples are similar (ca. 134.0 eV) except for the supported sample with 18% VPO loading. The P 2p BE of the 18% VPO/(H_3PO_4)-p-ZrO_2 sample is 133.5 eV; the 0.5-eV shift to lower energy could be a result of surface zirconium phosphate formation in close vicinity to VPO. In fact, the Zr $3d_{5/2}$ BEs of the supported samples are in the range of 183.1–183.5 eV (Table 2), approximately 1 eV higher than that of ZrO_2 (182.2 eV) but close to that of $Zr(OH)_4$ (183.6 eV) [69]. This observation suggests that as a result of H_3PO_4 treatment of ZrO_2, generation of zirconium phosphate occurs, especially on the surface of the support material. This deduction is also supported by (i) the closeness of the Zr $3d_{5/2}$ BE of 36% VPO/ZrO_2 (182.4 eV) to that of ZrO_2 (182.2 eV) [69] and (ii) the surface P/V atomic ratios depicted in Table 2. For the unsupported VPO sample, the P/V ratio is 1.4, showing slight enrichment of P element on the surface, as commonly observed on supported and unsupported VPO catalysts [1,10,32,33,47]. However, the high P/V atomic ratios (2.4–2.9) observed over the 18–45% VPO/(H_3PO_4)-p-ZrO_2, 36% VPO/(H_3PO_4)-ZrO_2, and 36% VPO/ZrO_2 samples are uncommon. In those H_3PO_4-treated samples, the extra presence of P is likely due to the coexistence of surface zirconium phosphate and VPO species. In 36% VPO/ZrO_2, however, the high surface P/V ratio could result from amorphous nature of dispersed VPO on the support. Early studies indicated that an "excess" amount of surface P may stabilize the pyrophosphate phase, favoring MA formation [1,70]. We propose that surface zirconium phosphate in the present study could have a similar effect, as we discuss in Section 3.2.1. In situ XPS studies of working VPO catalysts revealed that the surface P/V and O/V atomic ratios deviate with variations in feed composition and reaction temperature, suggesting that for MA formation from n-butane, the complexity involved demands active sites of varying natures [28].

The atomic ratio of surface zirconium to vanadium can be examined as a function of VPO coverage [32,38]. As shown in Table 2, the surface Zr/V atomic ratios of 18–45% VPO/(H_3PO_4)-p-ZrO_2 and 36% VPO/(H_3PO_4)-ZrO_2 are essentially the same (0.5–0.7). This is not so for VPO/SBA-15, however, in which the surface Si/V ratio decreases drastically with increasing VPO loading [40]. The surface Zr/V ratio of 36% VPO/ZrO_2 (2.2) is significantly higher than those of H_3PO_4-treated samples, suggesting that the dispersion of VPO on the two types of catalysts should be rather different. As pointed out earlier, the VPO dispersion on H_3PO_4-treated zirconia is fairly uniform and likely to be in the form of a thin layer. Such a manner of dispersion is probably an outcome of a unique interaction between VPO and surface zirconium phosphorate across the catalyst surface. The similar surface concentrations of V and P elements detected over 18–45% VPO/(H_3PO_4)-p-ZrO_2 (Table 2) supports the foregoing presumption. In fact, the TEM images of the 36% VPO/(H_3PO_4)-p-ZrO_2 sample (Figs. 1E and 1F) corroborate the results of XPS analysis. On the other

Table 2
XPS results of bulk VPO and VPO/(H_3PO_4)-p-ZrO_2 of different loadings

Sample	V $2p_{3/2}$ (eV)	P 2p (eV)	O 1s (eV)	Zr $3d_{5/2}$ (eV)	Surface composition (atom%)				Atomic ratio	
					V	P	O	Zr	P/V	Zr/V
Bulk VPO	517.0	134.0	531.3	–	11.4	16.3	72.3	–	1.4	–
45% VPO[a]	517.2	133.9	531.2	183.1	6.5	16.7	72.8	4.0	2.6	0.6
36% VPO[a]	517.1	134.1	531.5	183.5	6.9	16.3	73.0	3.7	2.4	0.5
27% VPO[a]	516.8	133.9	531.4	183.5	7.1	16.7	72.9	3.3	2.4	0.5
18% VPO[a]	516.9	133.5	531.3	183.2	5.8	17.1	73.1	3.9	2.9	0.7
36% VPO[b]	516.7	133.6	531.4	183.3	6.1	16.5	73.7	3.7	2.7	0.6
36% VPO[c]	516.8	133.8	531.1	182.4	5.1	12.0	71.5	11.4	2.4	2.2

[a] In VPO/(H_3PO_4)-p-ZrO_2.
[b] In VPO/(H_3PO_4)-ZrO_2.
[c] In VPO/ZrO_2.

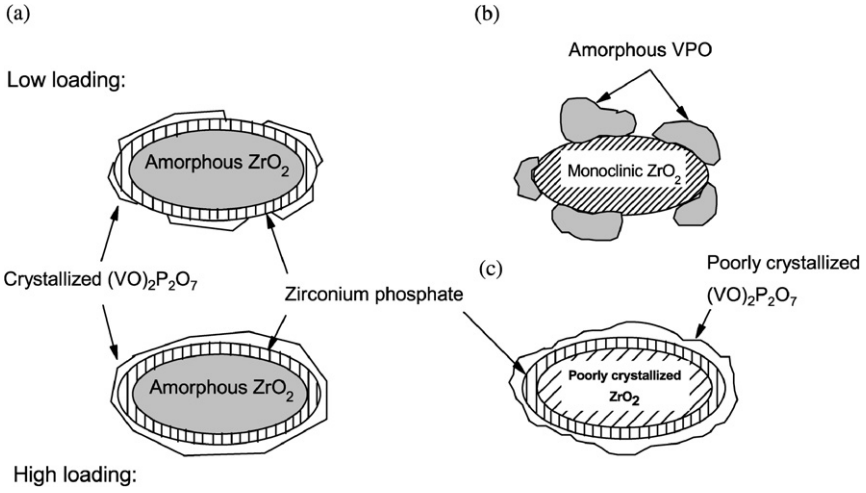

Scheme 1. Schematic illustration of VPO dispersion over (a) VPO/(H_3PO_4)-p-ZrO_2; (b) VPO/ZrO_2; (c) VPO/(H_3PO_4)-ZrO_2.

hand, the VPO dispersion on monoclinic ZrO_2 is poor, possibly a result of unfavorable interaction between the amorphous VPO and monoclinic ZrO_2.

Based on the results of various characterizations, a schematic illustration of the VPO dispersion over different supports is shown in Scheme 1.

3.2. Catalytic performance

3.2.1. The effect of H_3PO_4 treatment

The catalytic performance of unsupported VPO and the supported VPO catalysts is shown in Figs. 5A–5D. In the case of MA generation from n-butane over unsupported VPO, the typical n-butane conversion and MA selectivity at 400 °C are 93.6% and 72.1 mol%, respectively (Fig. 5A). As for the 36% VPO/ZrO_2 catalyst, the n-butane conversion and MA selectivity under similar reaction conditions are 54.0% and 28.6 mol%, respectively, giving a maximum MA yield of just 15.5 mol% (Fig. 5B). The poor generation of MA can be ascribed to the low reactivity of lattice oxygen (Fig. 4A) and the absence of crystalline vanadyl pyrophosphate phase (Fig. 2A). Over the 36% VPO/(H_3PO_4)-ZrO_2 catalyst, the n-butane conversion and MA selectivity are 54.6% and 58.9 mol%, respectively, giving an MA yield of 32.2 mol%. Over the 36% VPO/(H_3PO_4)-p-ZrO_2 catalyst, the n-butane conversion and MA selectivity are 89.1% and 68.8 mol%, respectively, giving a MA yield of 61.2 mol%. Compared with the activities reported over various supported VPOs, a MA yield of 61.2 mol% is significant and the best achieved so far [31–40,51,64].

Fig. 6 plots MA selectivities over 36% VPO/(H_3PO_4)-p-ZrO_2, 36% VPO/(H_3PO_4)-ZrO_2, and 36% VPO/ZrO_2 as a function of n-butane conversion. The MA selectivities decrease with increasing butane conversion over the three catalysts. However, at butane conversion of 45–90%, MA selectivity of 36% VPO/(H_3PO_4)-p-ZrO_2 (68–88 mol%) is higher than that of 36% VPO/(H_3PO_4)-ZrO_2 (48–60 mol%) and much higher than that of 36% VPO/ZrO_2 (10–34 mol%). Butane conversion of 90–100% can be achieved on 36% VPO/(H_3PO_4)-p-ZrO_2. The deep oxidation of reactant and product on this active catalyst becomes more significant at >90% butane conversion, resulting in a drastic decline in MA selectivity. At n-butane conversion of 40–70%, MA selectivity over 36% VPO/(H_3PO_4)-p-ZrO_2 reaches 75–88 mol%, significantly higher than those found over the VPO catalysts supported on conventional SiO_2 [32] as well as those on mesoporous MCM-41 and SBA-15 [39,40]. Within the temperature range of 380–400 °C, MA selectivity of 69–74 mol% and n-butane conversion of 74–89% are sustained, giving a MA yield of 55–61 mol%.

Arrhenius plots based on the turnover rates of MA over 36% VPO/(H_3PO_4)-p-ZrO_2 and 36% VPO/(H_3PO_4)-ZrO_2 are

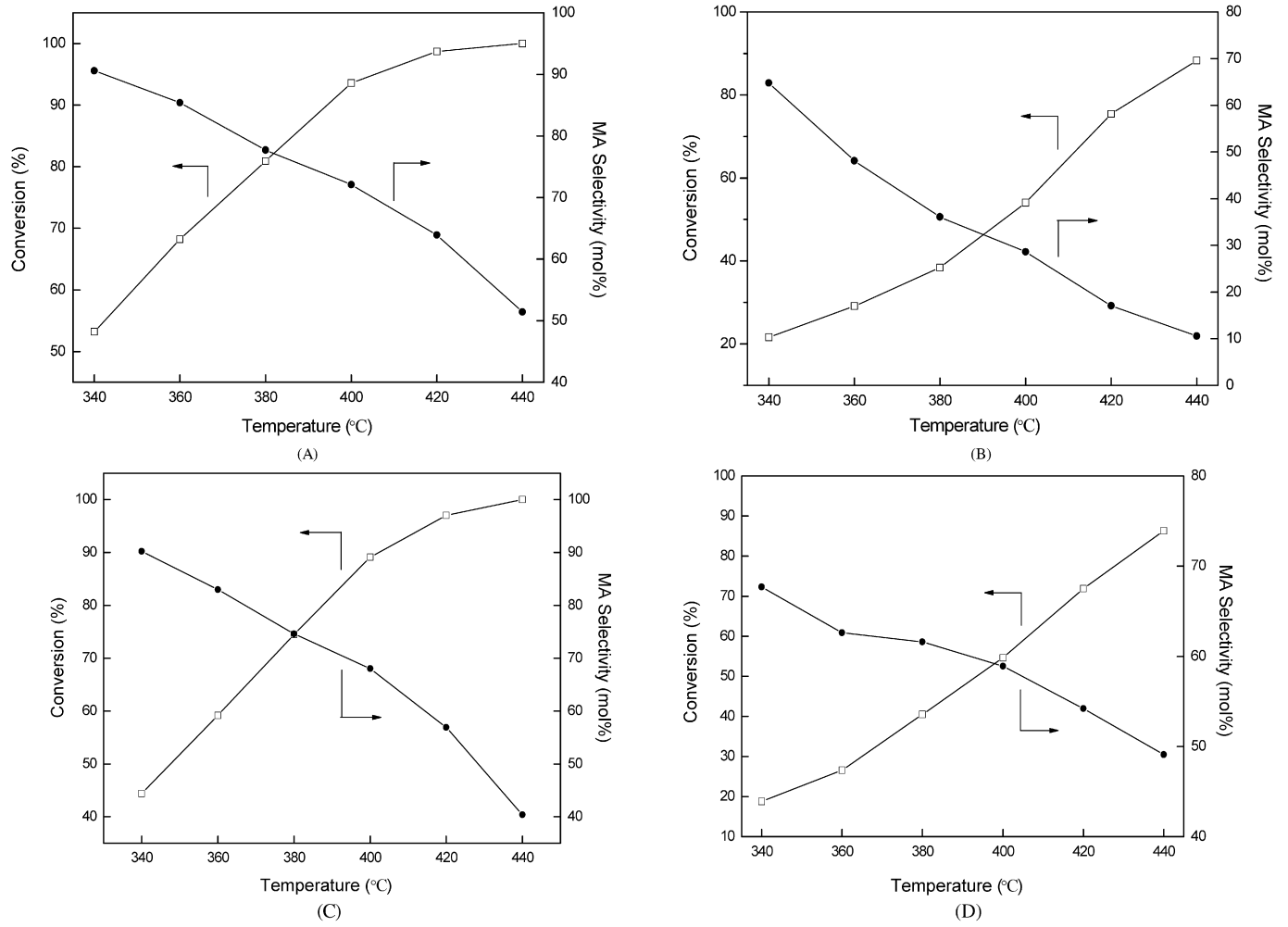

Fig. 5. n-Butane conversion and MA selectivity (GHSV = 1200 h^{-1}) as a function of reaction temperature over (A) unsupported VPO, (B) 36% VPO/ZrO_2, (C) 36% VPO/(H_3PO_4)-p-ZrO_2, and (D) 36% VPO/(H_3PO_4)-ZrO_2.

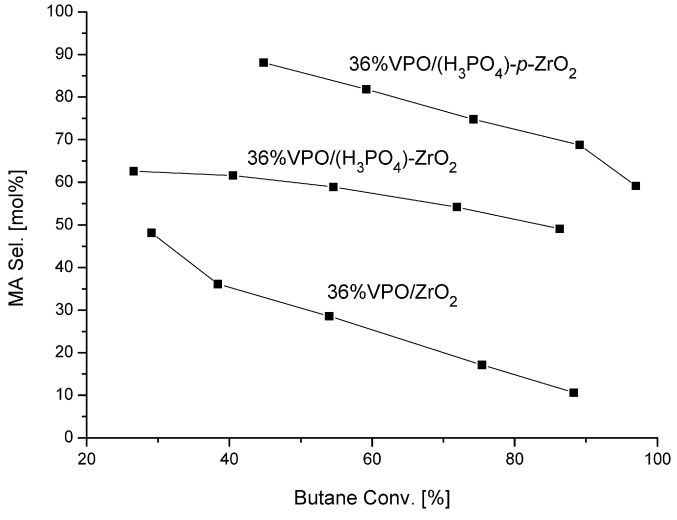

Fig. 6. MA selectivity over 36% VPO/(H_3PO_4)-p-ZrO_2, 36% VPO/(H_3PO_4)-ZrO_2, and 36% VPO/ZrO_2 as a function of conversion.

shown in Fig. 7. Assuming that the measured surface areas of these two samples equal that of VPO component, the apparent activation energies (E_a) are estimated from the integral reaction rates obtained at constant SV and at typical butane conversions (at 65 ± 17% and 38 ± 14% for 36% VPO/(H_3PO_4)-p-ZrO_2 and 36% VPO/(H_3PO_4)-ZrO_2, respectively). The E_a values are 23.0 kJ/mol for 36% VPO/(H_3PO_4)-p-ZrO_2 and 61.4 kJ/mol for 36% VPO/(H_3PO_4)-ZrO_2, fitting well with the catalyst activities.

The influence of H_3PO_4 concentration (adopted in H_3PO_4 treatment) on catalyst performance is depicted in Table 3. The H_3PO_4 concentration most suitable for support treatment is 1.0 mol/L.

3.2.2. The effect of VPO loading and GHSV

Fig. 8 illustrates the effect of VPO loading on the performance of the VPO/(H_3PO_4)-p-ZrO_2 samples. At an identical reaction temperature of 400 °C, n-butane conversion first increases with increasing VPO loading (from 18 to 36%) and then decreases, remaining at 78% at a VPO loading of 45%. The MA selectivity increases to ca. 68 mol% with an increase in VPO loading from 18 to 36%. Similar results were found over VPOs supported on silica [32,64] and SBA-15 [40]. At low VPO loading, the support surface not covered by VPO may cause side reactions; in addition, more reactive oxygen adspecies may be

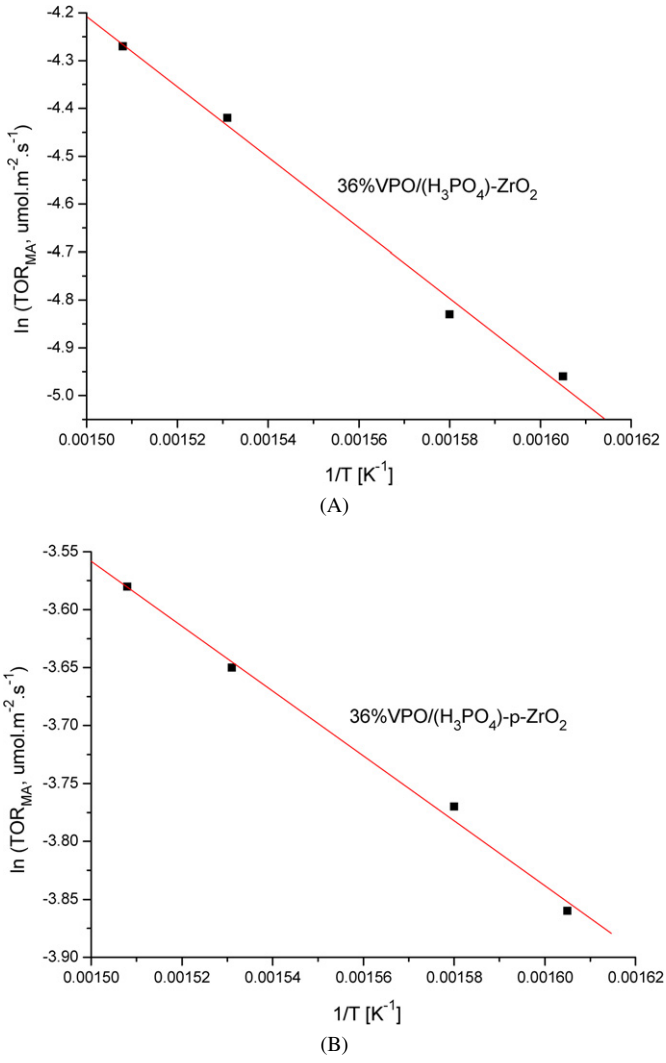

Fig. 7. The Arrhenius plots over (A) 36% VPO/(H_3PO_4)-ZrO_2 and (B) 36% VPO/(H_3PO_4)-p-ZrO_2 catalysts. The temperature range adopted for both 36% VPO/(H_3PO_4)-p-ZrO_2 and 36% VPO/(H_3PO_4)-ZrO_2 is 643 ± 20 K, at butane conversions of 65 ±17% and 38 ±14%, respectively.

Table 3
Effect of H_3PO_4 concentration adopted in H_3PO_4-treatment on catalyst performance

H_3PO_4 concentration	Temperature (°C)	C_{butane} (mol%)	S_{MA} (mol%)	Y_{MA} (mol%)
0.5 mol/L	380	60.6	54.2	32.8
	400	76.6	42.8	32.7
1.0 mol/L	380	74.5	74.5	55.5
	400	89.1	68.8	61.2
1.5 mol/L	380	67.5	34.0	22.9
	400	79.4	27.0	21.5

generated on the VPO component of smaller dimensions [71]; consequently, MA selectivity is low. At a high VPO loading of 45%, MA selectivity decreases. As shown by the XRD, Raman, and TPR characterization findings, an increase in VPO loading from 36 to 45% produces significant changes in phase composition, relative content of vanadyl pyrophosphate/orthophosphate

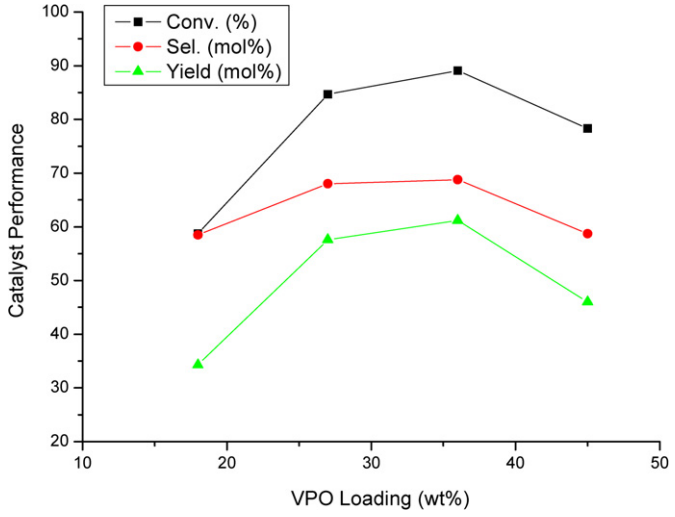

Fig. 8. The effect of VPO loading on the catalytic performance (at 400 °C) of serial VPO/(H_3PO_4)-p-ZrO_2 samples (at GHSV = 1200 h^{-1}).

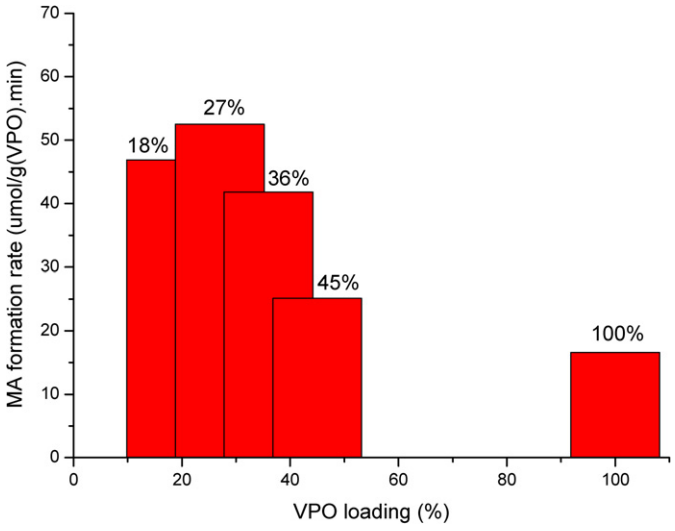

Fig. 9. MA formation rate (at 400 °C) over VPO/(H_3PO_4)-p-ZrO_2 catalysts on the basis of per unit mass of VPO component.

species, and reduction behavior of the VPO/(H_3PO_4)-p-ZrO_2 catalysts. Such alterations in catalyst characteristics should account for the observed difference in performance. As shown in Fig. 9, the MA formation rate at 400 °C, on the basis of per unit mass of VPO, decreases with increasing VPO loading and is notably higher than those derived over VPOs supported on SBA-15 [40] and fumed SiO_2 [64]. It can be envisaged that due to the higher dispersion of VPO at lower loadings, more active sites are available for the reaction on a "per unit mass" basis of VPO component.

Finally, the effect of GHSV on performance of the 36% VPO/(H_3PO_4)-p-ZrO_2 catalyst was studied; the results are illustrated in Fig. 10. It can be seen that n-butane conversion declines from 89.1 to 60.2% with increasing GHSV in the range of 1200–3000 h^{-1}, whereas MA selectivity first increases modestly from 68.8 to 71.2 mol% and then essentially remains unchanged with increasing GHSV. With due consideration of

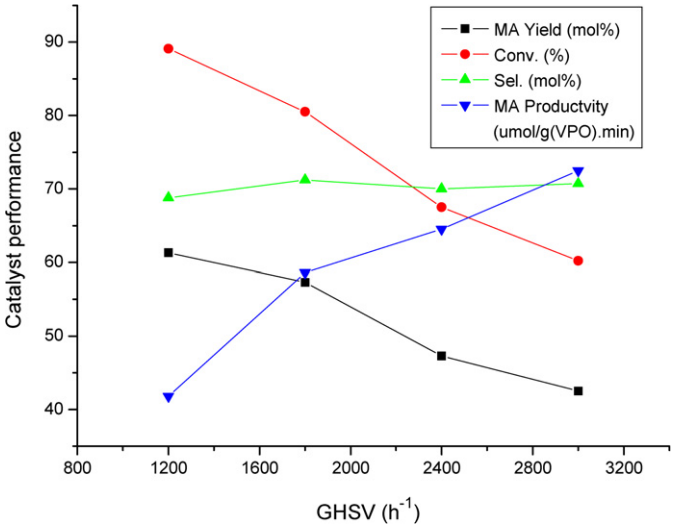

Fig. 10. The effect of gas hourly space velocity (GHSV) on the performance of catalyst 36% VPO/(H_3PO_4)-*p*-ZrO_2 (at 400 °C).

such factors as butane consumption, apparent MA yield, and MA productivity, the GHSV most suitable for the target reaction is 1800 h^{-1}.

Correlating the results of performance with those of characterization provides a structure–performance relationship. Good performance is closely related to the following factors: (i) appropriate phase composition (crystalline vanadyl pyrophosphate predominating on amorphous ZrO_2) [72], (ii) a small fraction of vanadyl orthophosphate species [73], (iii) higher coverage and reactivity of the VPO component, and (iv) a unique synergetic interaction between VPO and surface zirconium phosphorate.

4. Conclusion

In the present study, zirconia was used to support VPO for the partial oxidation of *n*-butane to MA. When ZrO_2 is used directly as support, the derived VPO/ZrO_2 catalyst shows rather poor performance. Over a VPO catalyst supported on ZrO_2 pretreated with phosphoric acid, an excellent MA yield is possible. The method of H_3PO_4 treatment has an affect on the nature and consequently the performance of the catalysts. Only VPO loaded on H_3PO_4-treated "dried ZrO_2 precursor" before calcination has excellent performance. At 400 °C, MA yield as high as 61 mol% can be obtained over the 36 wt% VPO/(H_3PO_4)-*p*-ZrO_2 catalyst, the best found to date over similar types of supported VPOs. We find that the good performance is strongly dependent on such critical structural features as phase composition of both VPO component and support, content of vanadyl orthophosphate species, and coverage and reactivity of the VPO component. It should be noted that certain structural features of the catalyst are significantly affected by the unique synergism between VPO and surface zirconium phosphorate on zirconia substrate of structural irregularity (from near amorphous to crystalline).

Acknowledgments

This work was supported by the RGC, Hong Kong Special Administration Region (Grant HKBU 200303). The research activities conducted at NJU were financed by the MSTC (Grant 2000048009).

References

[1] S.K. Hodnett, Catal. Rev. 27 (1985) 373.
[2] M. O'Connor, B.K. Hodnett, Appl. Catal. 42 (1988) 91.
[3] Y. Kamiya, S. Ueki, N. Hiyoshi, N. Yamamoto, T. Okuhara, Catal. Today 78 (2003) 281.
[4] J.B. Benziger, V. Guliants, S. Sundaresan, Catal. Today 33 (1997) 49.
[5] I.J. Ellison, G.J. Hutchings, M.T. Sananes, J.C. Volta, Chem. Commun. (1994) 1093.
[6] H.S. Horowitz, C.M. Blackstone, A.W. Sleight, G. Teufer, Appl. Catal. 38 (1988) 193.
[7] N. Hiyoshi, N. Yamamoto, T. Okuhara, Chem. Lett. (2001) 484.
[8] G. Busca, F. Cavani, G. Centi, F. Trifiro, J. Catal. 99 (1986) 400.
[9] V.V. Guliants, J.B. Benziger, S. Sundaresan, I.E. Wachs, J.M. Jehng, J.E. Roberts, Appl. Catal. A 28 (1996) 275.
[10] X.S. Wang, L.J. Xu, X. Chen, W.J. Ji, Q.J. Yan, Y. Chen, J. Mol. Catal. A 206 (2003) 261.
[11] M.J. Lorences, G.S. Patience, F.V. Díez, J. Coca, Appl. Catal. A 263 (2004) 193.
[12] F. Garbassi, J.C.J. Bart, R. Tassinari, G. Vlaic, P. Lagarde, J. Catal. 98 (1986) 317.
[13] V.V. Guliants, S.A. Holmes, J.B. Benziger, P. Heaney, D. Yates, I.E. Wachs, J. Mol. Catal. A 172 (2001) 265.
[14] M. Ruitenbeek, J.A. van Dillen, A. Barbon, E.E. van Faassen, D.C. Koningsberger, J.W. Geus, Catal. Lett. 55 (1998) 133.
[15] K. Ait-Lachgar, A. Tuel, M. Brun, J.M. Herrmann, J.M. Krafft, J.R. Martin, J.C. Volta, M. Abon, J. Catal. 177 (1998) 224.
[16] C.J. Kiely, A. Burrows, G.J. Hutchings, K.E. Bere, J.C. Volta, A. Tuel, M. Abon, Faraday Discuss. 105 (1996) 103.
[17] G. Centi, F. Trifirò, J.R. Ebner, V.M. Franchetti, Chem. Rev. 88 (1988) 55.
[18] V.V. Guliants, J.B. Benziger, N.Y. Sundaresan, I.E. Wachs, Catal. Lett. 32 (1995) 379.
[19] G.J. Hutchings, J.A. Lopez-Sanchez, J.K. Bartley, J.M. Webster, A. Burrows, C.J. Kiely, A.F. Carley, C. Rhodes, M. Havecker, A. Knop-Gericke, R.W. Mayer, R. Schlogl, J.C. Volta, M. Poliakoff, J. Catal. 208 (2002) 197.
[20] R. Ebner, M.R. Thompson, Catal. Today 16 (1993) 51.
[21] M.T. Sananes-Schulz, A. Tuel, G.J. Hutchings, J.C. Volta, J. Catal. 166 (1997) 388.
[22] V.V. Guliants, J.B. Benziger, S. Sundaresan, I.E. Wachs, J.M. Jehng, J.E. Roberts, Catal. Today 28 (1996) 275.
[23] N. Hiyoshi, N. Yamamoto, N. Ryumon, Y. Kamiya, T. Okuhara, J. Catal. 221 (2004) 225.
[24] N.H. Batis, H. Batis, A. Ghorbel, J.C. Vendrine, J.C. Volta, J. Catal. 128 (1991) 248.
[25] (a) G.J. Hutchings, C.A. Desmartin, R. Olier, J.C. Volta, Nature 368 (1994) 411;
(b) M. Conte, G. Budroni, J.K. Bartley, S.H. Taylor, A.F. Carley, A. Schmidt, D.M. Murphy, F. Girgsdies, T. Ressler, R. Schloge, G.J. Hutchings, Science 313 (2006) 1270.
[26] G.J. Hutchings, R. Higgins, J. Catal. 162 (1996) 153.
[27] J.-M. Herrmann, P. Vernoux, K.S. Bere, M. Abon, J. Catal. 167 (1997) 106.
[28] H. Bluhm, M. Havecker, E. Kleimenov, A. Knop-Gericke, A. Liskowski, R. Schlogl, D.S. Su, Top. Catal. 23 (2003) 99.
[29] G.W. Coulston, S.R. Bare, H. Kung, K. Birkeland, G.K. Bethke, R. Harlow, N. Herron, P.L. Lee, Science 275 (1997) 191.
[30] M. Lopez-Granados, J.C. Conesa, M. Fernandez-Garcia, J. Catal. 141 (1993) 671.
[31] K.E. Birkeland, S.M. Babitz, O.K. Bethke, H.H. Kung, G.W. Coulston, S.R. Bare, J. Phys. Chem. B 101 (1997) 6895.

[32] R.A. Overbeek, A.R.C.J. Pekelharing, A.J. van Dillen, J.W. Geus, Appl. Catal. A 135 (1996) 231.
[33] R.A. Overbeek, P.A. Warringa, M.J.D. Combag, L.M. Visser, A.J. van Dillen, J.W. Geus, Appl. Catal. A 135 (1996) 209.
[34] V.A. Zazhigalov, Y.P. Zaitsev, V.M. Belousov, B. Partitz, W. Hanke, G. Ohlmann, React. Kinet. Catal. Lett. 32 (1986) 209.
[35] W.D. Harding, K.E. Birkeland, H.H. Kung, Catal. Lett. 28 (1994) 1.
[36] J. Marc, C.C. Ledoux, P.H. Cuong, T. Vincent, K. Kostantinos, M. Patrick, L. Jan, J. Catal. 203 (2001) 495.
[37] J.M.C. Buenoa, G.K. Bethkeb, M.C. Kung, H.H. Kung, Catal. Today 43 (1998) 101.
[38] W.Y. Nie, Z.Y. Wang, W.J. Ji, Y. Chen, C.T. Au, Appl. Catal. A 244 (2003) 265.
[39] W.Y. Nie, X.S. Wang, W.J. Ji, Q.J. Yan, Y. Chen, C.T. Au, Catal. Lett. 76 (2001) 3.
[40] X.K. Li, W.J. Ji, J. Zhao, Z.B. Zhang, C.T. Au, J. Catal. 238 (2006) 232.
[41] N.T. Do, M. Baerns, Appl. Catal. 45 (1988) 1.
[42] N.T. Do, M. Baerns, Appl. Catal. 45 (1988) 9.
[43] E.A. Lombardo, C.A. Sanchez, L.M. Cornaglia, Catal. Today 15 (1992) 407.
[44] D. Ye, A. Satsuma, A. Hattori, T. Hattori, Y. Murakami, Catal. Today 16 (1993) 113.
[45] F.B. Abdelouahab, R. Olier, N. Guilhaume, F. Lefebvre, J.C. Volta, J. Catal. 134 (1992) 151.
[46] F.J. Cabello Sanchez, J.A. Lopez-Sanchez, R.P.K. Wells, C. Rhodes, Catal. Lett. 77 (2001) 189.
[47] G. Landi, L. Lisi, J.C. Volta, Catal. Today 91–92 (2004) 275.
[48] Y. Kamiya, S. Ueki, N. Hiyoshi, N. Yamamoto, T. Okuhara, Catal. Today 78 (2003) 281.
[49] L.M. Cornaglia, C.A. Sanchez, E.A. Lombard, Appl. Catal. A 95 (1993) 117.
[50] W.J. Ji, L.J. Xu, X.S. Wang, Z. Hu, Q.J. Yan, Y. Chen, Catal. Today 74 (2002) 101.
[51] Z.Q. Zhou, H.Y. Xu, W.J. Ji, Y. Chen, Catal. Lett. 96 (2004) 221.
[52] M. Fernandez-Garcia, A. Iglesias-Juez, A. Martinez-Arias, A.B. Hungria, J.A. Anderson, J.C. Conesa, J. Soria, J. Catal. 221 (2004) 594.
[53] M.Y. Smirnov, G.W. Graham, Catal. Lett. 72 (2001) 39.
[54] A. Iglesias-Juez, A. Martinez-Arias, M. Fernandez-Garcia, J. Catal. 221 (2004) 148.
[55] I.A. Fisher, A.T. Bell, J. Catal. 178 (1998) 153.
[56] K.D. Cheng, A.T. Bell, J. Catal. 193 (2000) 207.
[57] Y. Usami, K. Kagawa, M. Kawazoe, Y. Matsumura, H. Sakurai, M. Haruta, Appl. Catal. A Gen. 171 (1998) 123.
[58] W.J. Shen, M. Okumura, Y. Matsumura, Appl. Catal. A Gen. 213 (2001) 225.
[59] K. Nakagawa, K. Anzai, N. Matsui, N. Ikenaga, T. Suzuki, Y.H. Teng, T. Kobayashi, M. Haruta, Catal. Lett. 51 (1998) 163.
[60] G.J.J. Bartley, R. Burch, Appl. Catal. 43 (1988) 141.
[61] J.P. Breen, J.R.H. Ross, Catal. Today 51 (1999) 521.
[62] V. Adeeva, J.W. de Haan, J. Jauchen, G.D. Lei, V. Schunemann, L.J.M. van de Ven, W.M.H. Sachtler, R.A. van Santen, J. Catal. 151 (1995) 364.
[63] H. Weiming, X. Yongde, Y. Yinghong, G. Zi, J. Catal. 196 (2000) 104.
[64] C.Y. Xiao, X. Chen, Z.Y. Wang, W.J. Ji, Y. Chen, C.T. Au, Catal. Today 93–95 (2004) 223.
[65] W.J. Ji, J.Q. Hu, Y. Chen, Catal. Lett. 53 (1998) 15.
[66] H. Igarashi, K. Tsuji, T. Okuhara, M. Misono, J. Phys. Chem. 97 (1993) 7065.
[67] P. Delichere, K.E. Bere, M. Abon, Appl. Catal. A Gen. 172 (1998) 295.
[68] V.I. Bukhtiyarov, Catal. Today 56 (2000) 403.
[69] T.L. Barr, J. Phys. Chem. 82 (1978) 1801.
[70] R.W. Wenig, G.L. Schrader, J. Phys. Chem. 90 (1986) 6480.
[71] M. Abon, J.C. Volta, Appl. Catal. A 157 (1997) 173.
[72] V.V. Guliants, Catal. Today 51 (1999) 255.
[73] J.C. Volta, Catal. Today 32 (1996) 29.